ACS APPLIED MATERIALS & INTERFACES

Research Article

www.acsami.org

Lightweight and Flexible Reduced Graphene Oxide/Water-Borne Polyurethane Composites with High Electrical Conductivity and Excellent Electromagnetic Interference Shielding Performance

Sheng-Tsung Hsiao,[†] Chen-Chi M. Ma,*[,†] Wei-Hao Liao,[†] Yu-Sheng Wang,[†] Shin-Ming Li,[†] Yu-Chin Huang,[†] Ruey-Bin Yang,[‡] and Wen-Fan Liang[§]

[†]Department of Chemical Engineering, National Tsing-Hua University, Hsin-Chu 30013, Taiwan, ROC

[‡]Department of Aerospace and Systems Engineering, Feng Chia University, Taichung 40724, Taiwan, ROC

[§]Department of Aeronautics and Astronautics, National Cheng Kung University, Tainan 70101, Taiwan, ROC

Supporting Information

ABSTRACT: In this study, we developed a simple and powerful method to fabricate flexible and lightweight graphene-based composites that provide high electromagnetic interference (EMI) shielding performance. Electrospun water-borne polyurethane (WPU) that featured sulfonate functional groups was used as the polymer matrix, which was light and flexible. First, graphene oxide (GO)/WPU composites were prepared through layer-by-layer (L-b-L) assembly of two oppositely charged suspensions of GO, the cationic surfactant (didodecyldimethylammonium bromide, DDAB)-adsorbed GO and intrinsic negatively charged GO, depositing on the negatively charged WPU fibers. After the L-b-L assembly cycles, the GO bilayers wrapped the WPU fiber matrix completely and revealed fine connections guided by the electrospun WPU fibers. Then, we used hydroiodic acid (HI) to obtain highly reduced GO (r-GO)/WPU composites, which exhibited substantially enhanced electrical conductivity (approximately 16.8 S/m) and, moreover, showed a high EMI-shielding effectiveness (approximately 34 dB) over the frequency range from 8.2 to 12.4 GHz.

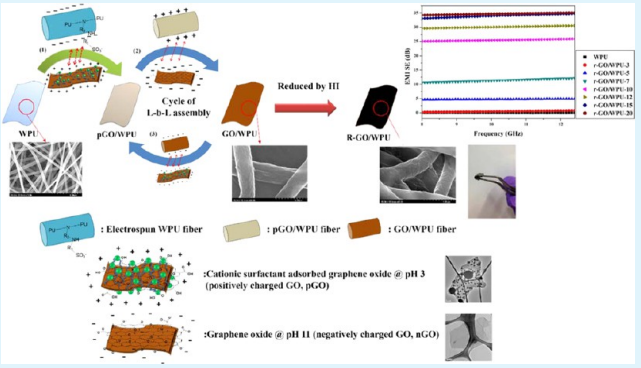

KEYWORDS: *graphene nanosheet, water-borne polyurethane, electromagnetic interference shielding, electrical conductivity, layer-by-layer assembly*

1. INTRODUCTION

Electronic devices that are currently being rapidly developed are packed with highly integrated circuits and exhibit high operational frequencies that induce electromagnetic interference (EMI). EMI not only impedes the functionality of electronic devices but also harms humans. Thus, EMI has emerged as a major concern in today's society, and substantial great effort has been devoted toward developing materials that provide high EMI shielding.[1] The frequency range of 8.2−12.4 GHz (X band) is used widely on military and communication applications, such as radar, telephone microwaves, and TV picture transmission.[2] Therefore, the shielding performance in X band is important. Metals and metallic composites have conventionally been used as shielding materials because they conduct electricity extremely well. However, the drawbacks associated with these materials include their weight, high corrodibility, and the difficulty of processing them. Therefore, electrical conductive polymer composites are considered favorable materials for developing effective EMI-shielding applications,[3,4] and these materials offer advantages including those of being light, flexible, resistant to corrosion, easy to process, and inexpensive, when compared to the conventional metallic materials. Shielding performance typically relies primarily on the electronic conductivity of the polymer composites, which is dominated by the filler's intrinsic conductivity, aspect ratio, and the connection of conductive fillers.[5]

Numerous carbon-based materials have been used as conductive fillers to fabricate conductive polymer composites,[6−8] including carbon particles, carbon fibers, carbon nanotubes, and graphene. Graphene is an one-atom-thick 2D layer of the sp^2 carbon lattice that has attracted considerable attention from both fundamental and applied research communities since it was discovered by Geim in 2004.[9] The extraordinary mechanical, electrical, and thermal properties of the graphene coupled with its high specific surface area have led

Received: April 21, 2014
Accepted: June 12, 2014
Published: June 12, 2014

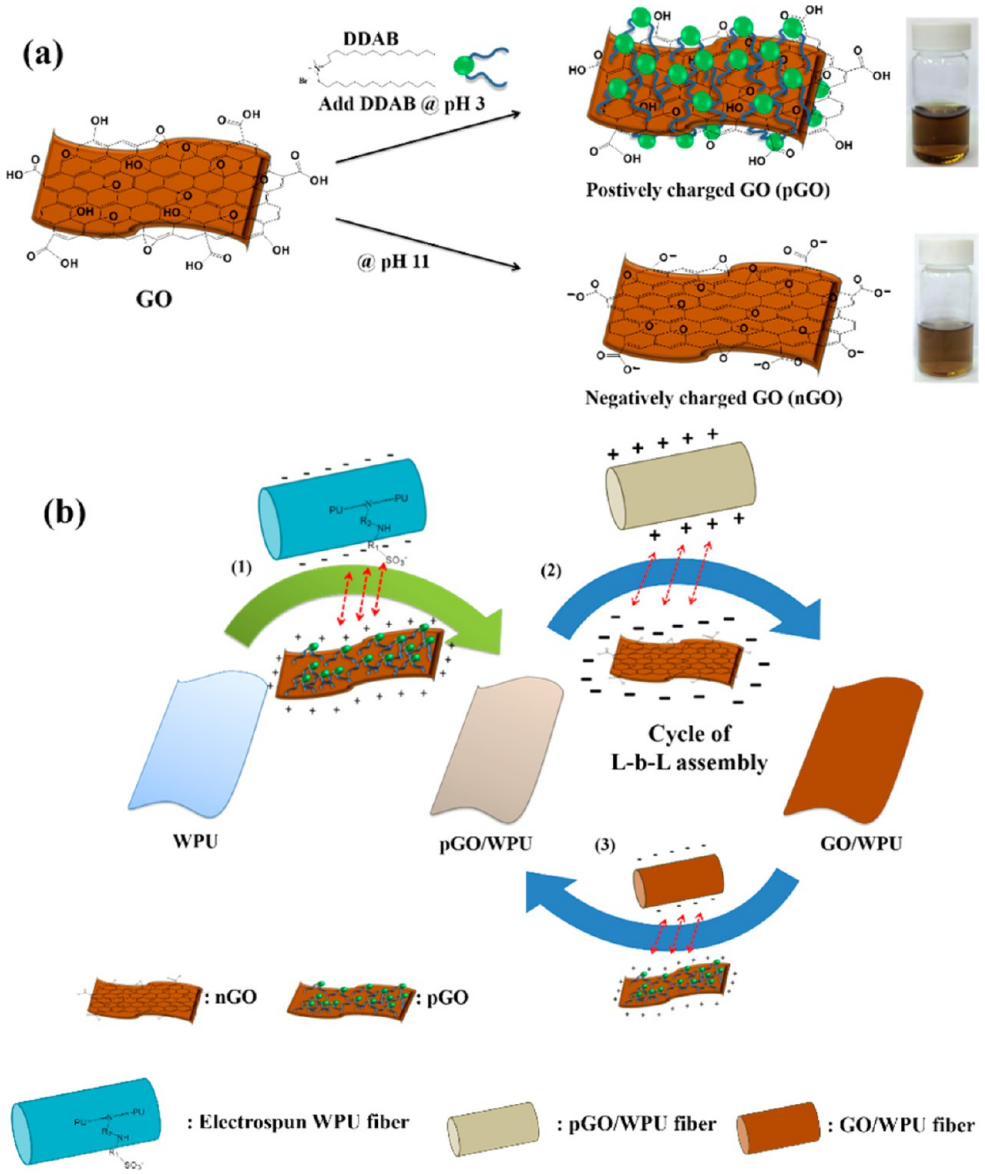

Figure 1. (a) Schematic representation of the procedure used to prepare the segments used in L-b-L assembly: positively charged segment, pGO, and negatively charged segment, nGO. (b) Schematic representation of the cycle of L-b-L assembly of pGO and nGO on the WPU fiber. The buildup sequence included three steps: (1) adsorption of WPU and pGO and formation of pGO/WPU; (2) adsorption of pGO/WPU and nGO. The first cycle of L-b-L assembly is completed when the GO/WPU composite is obtained. (3) The GO/WPU composite is repeatedly used in the next cycle of L-b-L assembly, which is repeated as necessary to obtain the desired times.

to the emergence of graphene as a promising nanofiller in multifunctional composites.[10,11] Early basic research in this field was based on the micromechanical cleavage of highly crystalline graphite to generate high-quality graphene, but recent efforts have turned to producing the graphene in a controlled scale and reproducible manner. Chemical reduced graphene oxide (r-GO) has been considered a promising method to produce graphene on a large scale.[12,13] Graphene oxide (GO), which is produced by the chemical oxidation of graphite, exhibits a layered structure featuring numerous oxygenated functional groups (hydroxyl (−OH), epoxy (−COC), carbonyl (−C═O), and carboxyl groups (−COOH)).[14] Because ionized carboxyl groups ($-COO^-$) occur on the edges of a GO layer, GO is hydrophilic and water-soluble.[15] However, the basal plane of a GO layer contains unoxidized benzene rings and hydrophobic polyaromatic island. Consequently, GO can be considered an amphiphilic substance featuring a hydrophobic basal plane and hydrophilic edges.[16] Because numerous sp^3 carbon atoms and a few sp^2 carbon atoms are present on the GO surface, electrons cannot be delocalized on GO surfaces, and therefore, GO can serve as an insulator.[17] However, for use in electronic applications, GO must be reduced to make it electrically active. Currently, hydrazine[12] and sodium borohydride[18] are commonly used as chemical reducing agents to effectively deoxygenate GO. However, during chemical reduction, additional functional groups are introduced and the graphitic structure of r-GO disintegrates, which severely degrades the electrical conductivity of r-GO.[19] Previous study indicated that GO reduced by hydroiodic acid (HI) exhibited highly electrical conductive;[19] thus, this method represents a favorable approach that can be used for reducing GO.

r-GO have been widely used as fillers in the fabrication of electrically conductive polymer composites.[10,11,20] In con-

ductive bulk-polymer composites, the r-GO are introduced into and randomly dispersed in the polymer matrix and are surrounded by the polymer's molecular chains. To exhibit a high EMI-shielding performance, the r-GO must form a conductive network inside the insulating polymer matrix.[6,21] Usually, a large amounts of r-GO are necessary. However, a high loading of r-GO can result in severe agglomeration and poor compatibility with polymer matrix, which increases the difficulty associated with processing the material and also compromises the mechanical performance of the polymer composite.[20] On the basis of our previous work,[22] we have provide a noncovalent modification to modify the r-GO by adsorption of cationic surfactant, which not only inhibits the restacking of r-GO but also improved the compatibility with the polymer matrix. However, the interaction of surfactant and GN will disappear resulted in an unstable dispersion during the preparation of polymer composites. Several groups have attempted to fabricate electrically conductive foam polymer composites.[23,24] Although foam composites can reduce the material's weight more effectively than bulk-polymer composites can, the electrical conductive network in the matrix is damaged during the foaming process, which exhibits a high intersheet junction contact resistance and limits EMI shielding performance.[25] Moreover, the poor mechanical property of a foam polymer restricts its application. Recently, a novel method has been proposed to prepare polymer composites by decorating r-GO or carbon nanotubes onto electrospun polymer fibers.[26,27] The fillers decorated on the fiber surface can effectively improve the properties of the composites, especially electrical conductivity. However, the compatibility of fillers and polymer fibers is often neglected, which can create problems: (1) controlling the quantity of the fillers decorated on the polymer fillers can be challenging; (2) the decoration process may be time-consuming, and such long processing time easily causes the aggregation of fillers because of strong van der Waals forces, limiting the reinforcement of fillers; and (3) the decorated fillers may peel off readily because of a poor interaction between fillers and polymer fibers.

The layer-by-layer (L-b-L) self-assembly technique is widely used to fabricate organic−inorganic polymer composites by exploiting the electrostatic attraction between oppositely charged components.[28,29] Recently, L-b-L assembly was used to fabricate graphene-based composites comprising poly(acrylic acid)-modified and poly(acrylamide)-modified r-GOs[30] or negatively charged r-GOs and positively charged modified r-GOs.[29] This process represents a simple, powerful, and effective approach that can be used to fabricate graphene-based polymer composites in which the type, size, morphology, and molecular structure are controlled. However, in these assembly methods, the positively or negatively charged r-GOs are grafted with molecules or polymers that disrupt electron transmission, which degrades the electrical conductivity of the r-GO and limits the conductivity of the polymer composite.

In this study, r-GO/waterborne polyurethane (WPU) composites were fabricated using a novel method. We used electrospinning to obtain a WPU matrix, which possessed a high surface area, making it a suitable matrix for use in the EMI polymer composite. Moreover, the intrinsic sulfonate functional groups grafted on the WPU polymer chain generated a negatively charged substrate that could be used in L-b-L assembly without further treatment[31] GO/WPU composites were generated through L-b-L assembly by using two oppositely charged GOs and the WPU matrix. As described in previous studies,[16,32] by controlling the pH of an aqueous GO suspension and by adsorbing a cationic surfactant, didodecyldimethylammonium bromide (DDAB), on the basal plane of GO, a positively charged GO (pGO) was obtained (Figure 1a). Conversely, the carboxylic functional groups on GO edges made the GO negatively charged (nGO) and exfoliated it homogeneously in aqueous solutions. The nGO and pGO were obtained by a simple method, and their structure was still completed. After completing the L-b-L assembly of pGO and nGO for cycles on the WPU fibers, the WPU fibers were finely covered by GO, which formed a GO network (Figure 1b). To improve the electrical conductivity of the GO/WPU composite, HI was used to reduce GO/WPU to the r-GO/WPU composite. Here, we focus on the orientation and interaction of r-GO on the WPU matrix during the L-b-L assembly process and discuss the influence of r-GO on electrical conductivity and EMI-shieling shielding performance.

2. EXPERIMENTAL SECTION

2.1. Materials. Nanographite plates (NGPs) were synthesized by using a chemical vapor deposition process supplied by Angstron Materials LLC, McCook Avenue Dayton, Ohio, U.S.A. The thickness of the NGPs was less than 100 nm. Potassium permanganate ($KMnO_4$), sodium nitrate ($NaNO_3$), hydrogen peroxide (H_2O_2), sulfuric acid (H_2SO_4), sodium borohydride ($NaBH_4$), HI, and diethanolamine (DEA) were obtained from Showa Chemical Co., Tokyo, Japan. Hexamethylene diisocyanate (HDI), DDAB, ammonium hydroxide (NH_4OH), and hydrochloric acid (HCl) were purchased from Tokyo Chemical Industry Co., Ltd., Tokyo, Japan. Hydrazine (N_2H_4) was received from Alfa Aesar GmbH & Co. KG, Karlsruhe, Germany. Poly(ethylene oxide) (PEO) (M_w = 900 000) were purchased from Acros Organics Co., New Jersey, U.S.A. Polycaprolactone diol (PCA) (M_w = 2000) was received from Sigma−Aldrich Co., LLC, St. Louis, U.S.A. YA-7720 (M_w = 2000, 96 wt %), the polyester based polyol, was obtained from Coating Chemical Industry Co., Ltd., Taichung, Taiwan. *N*-(Ethylene sulfonate sodium salt)ethylene diamine (EES-200L, 45 wt %) were obtained from Jiuh Yi Chemical Industry Co., Ltd., Taipei, Taiwan. Di-*n*-butyltin dilaurate (DBTDL) was received from Alfa Aesar Co., Ward Hill, U.S.A.

2.2. Preparation of nGO and pGO. GO was synthesized by modified Hummers method.[33,34] Nanographite (0.5 g) and $NaNO_3$ (0.375 g) were added in a three-necked 100 mL flask with H_2SO_4 (20 mL) and magnetically stirred at 0−3 °C in an ice bath. $KMnO_4$ (2.25 g) was added slowly into the mixture over 10 min with stirring and cooling to 0 °C. After it was stirred, for 2 h at 40 °C, the mixture became pasty and brownish. Then, the flask was placed in an oil bath at 70 °C to reduce the viscosity of the mixture, and 30 mL reverse osmosis water (RO water) was added inside slowly. After the mixture was cooled to room temperature, 375 mL H_2O_2 (5 wt %) was added to the resulting solution to reduce the residual permanganate and MnO_2 to soluble $MnSO_4$, and the suspension turned bright yellow. The product was purified cycle by repeating the following procedure cycle for 10 times: removal of supernatant liquid, addition of a mixed aqueous solution of H_2O_2 (5 wt %), and centrifugation at 10 000 rpm for 40 min. After 10 complete cycles, GO was dissolved in RO water again. Finally, the GO, well-dispersed in RO water, was obtained. Because of the carboxyl groups on the GO surfaces the resulting nGO is negatively charged in alkali environment (pH value > 7). The pGO solution was synthesized by adding DDAB (30 mg) into the GO solution (10 mg/10 mL) in acidic surrounding. The mixture was ultrosonicated at low energy (12 W, 55 kHz) for 2 h to obtain good homogeneity. Then, pGO solution of dark brown color was acquired. The schemes of preparation of nGO and pGO are shown in Figure 1a.

2.3. WPU Solution Preparation. At first, YA-7720 (30 g), PCA-2000 (20 g), and HDI (5.04 g) were put into a four-necked 500 mL reactive vessel equipped with a mechanical stirrer, which was placed in an oil bath at 90 °C. Reaction was started by the addition of 0.005 g of

catalyst DBTDL. When the prepolymer reaction was completed, the temperature was cooled to 40 °C, and acetone was added to the vessel to dissolve the prepolymer until totally dissolved. Then, the chain extender agent composed of hydrazine (0.08 g), EES-200L (0.845 g), and DEA (0.054 g) were dripped into the vessel at 40 °C for 1 h. Then, RO water (100 mL) was added dropwise with stirring at 30 °C. Finally, the WPU aqueous solution was obtained with a concentration of 35 wt %.

2.4. Electrospinning Process. The nanofiber electrospinning unit (NEU) from Kato Tech Co., Ltd. (Japan), was used to setup the electrospinning process. All the ES parameters were kept constant. According to the previous study,[35] PEO was used as the template polymer for WPU electrospinning. First, PEO was dissolved in distilled water by magnetic stirring at 50 °C. Then, PEO solution was added to the WPU solution for adjusting to the 30/70 PEO/WPU weight ratio. After that, the WPU solution was fed into a 10 mL syringe with a stainless steel needle (18 gauge needle). The flow rate of WPU solution was set at 0.2 mL/h. An applied voltage of 10 kV was setup directly to the needle, and the distance between needle and the collector was kept at approximately 15 cm. An aluminum foil was used as the collecting electrode, and the resulting fibers were collected on the aluminum foil to produce a sheet of nonwoven fabric. Finally, the electrospun WPU sheet was put into distilled water for at room temperature 24 h, and the PEO was removed.

2.5. L-b-L Assembly of pGO and nGO on WPU Fibers. The overall process of L-b-L deposition, as shown in Figure 1b, consists of a cyclic repetition of following steps. a sheet of 2 cm × 2 cm × 1 mm WPU mat was immersed into a pGO solution (1 wt %) for 1 min. Then, the pGO/WPU was rinsed with distilled water thoroughly for 30 s and dried with air flow. After that, the pGO/WPU was put into the nGO solution (1 wt %) and immersed it for 1 min. Again, the dipped sheet was rinsed with DI water thoroughly for 30 s and dried with air flow. Upon completing the above steps, a single bilayer GO was formed on the WPU fibers (GO/WPU). Furthermore, above cycle was repeated until the desired number (1, 3, 5, 7, 10, 15, 20 times, called GO/WPU-1, 3, 5, 7, 10, 15, 20) of bilayers was deposited.

2.6. Fabrication of r-GO/WPU Composites. HI was chosen to reduce GO. HI was placed in an oven at 100 °C. The GO/WPU composite was dipped into the HI for 10 s and subsequently dried in an oven. After that, the specimen was washed with dipping in the DI water and acetone for 5 min, and dried overnight in vacuum at room temperature. Finally, an r-GO/WPU composite was obtained.

2.7. Characterization. Transmission electron microscope (TEM) observation was performed using a JEM-2100 microscope (JEOL, Limited, Tokyo, Japan) operating at an accelerating voltage of 200 kV. The ζ potential measurements of the samples in an aqueous dispersion were carried out at room temperature using a Malvern Zetasizer Nano-ZS system, and detail information about the characterization is shown in Supporting Information. Elemental composition analysis was conduct with a high resolution X-ray Photoelectron Spectrometer (XPS) (ESCA pHI 1600, Physical Electronics, U.S.A.). The microstructure was characterized by using an Ultima IV multipurpose X-ray diffraction (XRD) system (Rigaku Co., Sendagaya, Shibuya-Ku, Tokyo, Japan) with Cu Kα radiation (λ = 1.54051 Å) at the scan rate of 1° min^{-1}. With intervals from 2° to 40°. Raman spectra were recorded from 1000 to 2000 cm^{-1} in a Stellar-PRO confocal Raman microscopy system (MODU-LASER, LLC), and the laser wavelength was 488 nm. Morphology observations of polymer composites were imaged by a scanning electron microscope (SEM, S-4200 microscope (Hitachi Limited, Tokyo, Japan)), with a 15 kV accelerating voltage, and the low electrical conductivity samples were coated with 5 nm thick layer of gold (Cressington 208HR sputter coater) to limit the charging effects under investigation. Thermal degradations of WPU, r-GO, and r-GO/WPU composites were investigated by a thermogravimetric analyzer (TGA) (Hi-Res TGA 2950, TA Instruments, U.S.A.) from room temperature to 650 °C with a heating rate of 10 °C/min under N_2 atmosphere (100 mL/min).The volume electrical resistance of moderately electrical conductive polymer composite was carried out using a standard four-point probe method (FPP-5000, Miller Design Co., Woodside Rd, Woodside, Canada). The average value was obtained from five measurements for each sample. As to low electrical conductive polymer composite, the volume resistance was measured by an SME-8311 megohmmeter (Dkk-Toa Co., Tokyo, Japan) with 20 s charge time and 100 V of current stress. An average value was achieved from five measurements for each sample. EMI shielding measurements were conducted in the frequency range of 8.2−12.4 GHz (X band) at room temperature by using a 8501C Vector Network Analyzer. The measured samples were cut into a coaxial circle with 3.00 mm of inner diameter, 7.00 mm of outer diameter, and 2.00 mm of thickness. The total EMI shielding effectiveness (SE) of shielding material is the sum of reflection (SE_R), absorption (SE_A) and multiple reflection (SE_M). The reflection is related to the impedance mismatch between air and absorber; the absorption is resulted from the energy dissipation of electromagnetic radiation; and the multiple reflection is induced by the scattering effect of the inhomogeneity in the material.[36] The total EMI SE (SE_{total}) is defined as the logarithmic ratio of incoming (P_i) to outgoing power (P_o) of radiation.[37]

$$SE_{total} = 10 \log(P_i/P_o) = SE_A + SE_R + SE_M$$

When SE_{total} > 10 dB, SE_M can be neglected,[38] and it is usually assumed that

$$SE_{total} \approx SE_A + SE_R$$

The S_{11} (or S_{22}) and S_{12} (or S_{21}) parameters of the two-port network system stand for the reflection and transmission coefficient. Transmittance (T), reflectance (R), and absorbance (A) through the shielding material were analyzed by the S parameters, which can be described as

$$T = |S_{12}|^2 = |S_{21}|^2$$

$$R = |S_{11}|^2 = |S_{22}|^2$$

$$A = 1 - R - T$$

The effective absorbance can be expressed as[36]

$$A_{eff} = (1 - R - T)/(1 - R)$$

As for the power of the effective incident electromagnetic radio inside the shielding material, the reflectance and effective absorbance can be expressed as

$$SE_R = -10 \log(1 - R)$$

and

$$SE_A = -10 \log(1 - A_{eff}) = -10 \log[T/(1 - R)]$$

3. RESULTS AND DISCUSSION

3.1. Characterization of nGO and pGO. The structure of layered materials can be determined by analyzing XRD patterns. As shown in Figure 2, the XRD spectrum of NGP displayed a sharp and narrow peak (002) in the 2θ range of 26.5°, indicating a well-ordered lamellar structure featuring an interlayer spacing of 3.36 Å. After oxidation, the XRD pattern of GO exhibited a peak in the 2θ range of 10.61°, corresponding to an interlayer spacing of GO of 8.334 Å, which was larger than the interlayer spacing of NGP. Since a large amount of oxygenated functional groups were bonded on the GO surface and intercalated into the interlayer space, generating an exfoliated structure. These results showed that exfoliated GO was obtained using the modified Hummers method.

To complete the L-b-L assembly of the GO bilayers on the electrospun WPU matrix, oppositely charged GOs were necessary. GO behaves like a surfactant because it contains hydrophilic carboxylic functional groups and a hydrophobic basal plane.[16] The carboxylic functional groups present along GO edges make GO negatively charged (nGO) and exfoliate

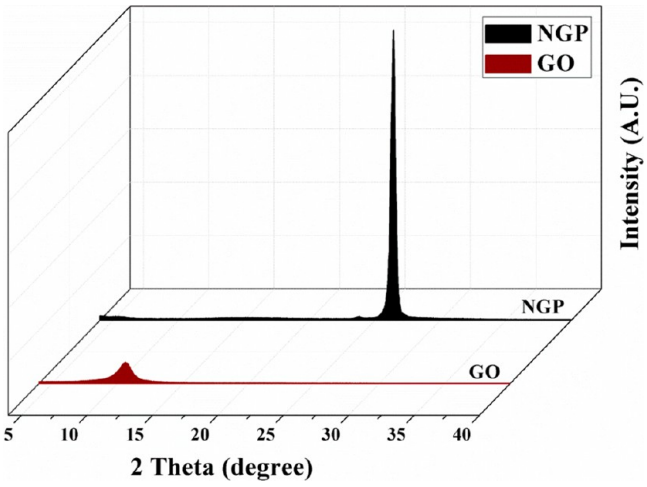

Figure 2. XRD results of NGP and GO.

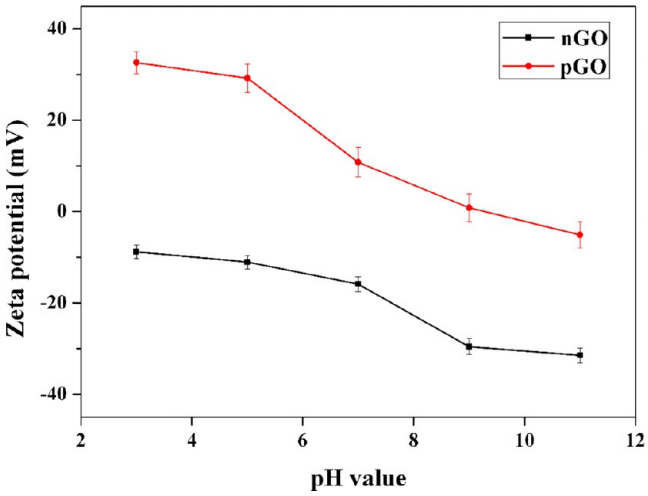

Figure 3. Zeta potential investigations of nGO and pGO as a function of various pH value of solution.

them homogeneously in aqueous solutions, especially in an alkaline environment.[32] Conversely, to obtain positively charged GO, the cationic surfactant, DDAB, was added to the GO suspension (pGO). The hydrophobic tailed parts of DDAB adsorbed onto the hydrophobic basal plane of GO, and the exposed hydrophilic head groups imparted the positive charges to pGO. However, the ionization of the carboxylic functional groups on the GO edges plays a key role in controlling the charge of pGOs. By changing the pH of a GO suspension, the degree of ionization of carboxylic functional groups can be controlled readily. When the pH of a GO suspension is increased, the carboxylic functional groups ionize easily and increase the negative charge of GO; however, it is hard to obtain positively pGO by adding DDAB. At a low pH, poor ionization of the carboxylic functional groups on GO edges reduces the negative charge and hydrophilicity of GO, which is more suitable for fabricating pGO than using GO at a high pH. Therefore, to obtain highly charged nGO and pGO effectively, controlling the pH of the nGO and pGO suspension was critical.

Zeta potential is a parameter that can accurately indicate the charge of a colloidal solution.[39,40] When we varied the pH of the nGO and pGO solutions by adding HCl and NH_4OH, the zeta potential values became increasingly negative with increasing pH in both nGO and pGO solutions (Figure 3). This was because the alkaline environment increased the number of carboxylic functional groups that ionized to negative −COO− functional groups on the GO edges. Moreover, the less negative zeta potential of nGO was observed when disperse at low pH, because the ionization of the carboxylic functional groups on the GO edges was inhibited. However, the zeta potential of nGO increased slightly when the pH of the nGO solution was greater than 9, which was because most carboxylic functional groups were ionized. In the case of the pGO solution, the zeta potential became increasingly positive charge with decreasing pH. This suggested that inhibiting the ionization of the carboxylic functional groups on the GO edges reduced the hydrophilicity of GO,[32] which increased the ease with which DDAB was adsorbed on the hydrophobic basal plane of GO to make the zeta potential increasingly positive. As in the case of nGO, the zeta potential of pGO did not increase markedly when the pH was 3, which suggested that DDAB had adsorbed on the GO surface completely. To promote effective L-b-L assembly, a large zeta potential difference between nGO and pGO was necessary; thus, the nGO solution at pH 11 (−31.47 mV) and pGO solution at pH 3 (32.64 mV) were selected for use in L-b-L assembly.

To further characterize the adsorption of DDAB on GO, we used TEM to investigate the morphologies of GO and pGO. Both GO and pGO exhibited unique 2D structures featuring large aspect ratios. As shown in Figure 4a, GO exhibited a lamellar structure, which indicated that we had obtained an exfoliated GO; a smooth, mat-like structure was observed because oxygenated functional groups were present on the GO surface.[41] Compared with GO, pGO displayed a rougher structure featuring numerous dark zones (Figure 4b), which indicated that DDAB was adsorbed on the GO surface. Moreover, because the long alkyl chains (hydrophobic parts) of DDAB easily became entangled and coiled during solvent evaporation, globular structures were generated on the GO surface. As shown in Figure 4c, the pGO was fully adsorbed by DDAB, and the excess DDAB even formed numerous micelles on the pGO surface.

3.2. Characterization of GO and r-GO. Next, XPS was used to analyze the chemical compositions of C−C/C−O bonding of GO and r-GO. Figure 5 illustrates the C 1s XPS spectra depicting the detailed surface composition of GO and r-GO. The C 1s spectrum of GO (Figure 5a) shows that GO contained a small fraction of carbon/carbon bonding (aromatic C═C and aliphatic C−C) and a large amount of oxygen functional groups arising from epoxy carbon C−O−C, hydroxyl carbon C−O, carbonyl carbon C═O, and carboxylate carbon O−C═O.[15,42] A lower fraction of aromatic C═C bonding was detected compared with aliphatic C−C bonding, which demonstrated that the C═C structures had been damaged by the oxidation that occurred when the modified Hummers method was used. The results in Figure 5a indicate that the epoxy functional groups were the most common groups existing on the GO basal plane, which agrees with previous studies.[43] Furthermore, the detection of the O−C═O functional group on GO supported the results of the zeta-potential measurements. The C 1s XPS spectrum of r-GO is presented in Figure 5b. After GO was reduced using HI, the oxygen functional groups were almost eliminated, especially the epoxy group, and the aromatic C═C bond became dominant. Moreover, the appearance of a peak at 289.9 eV, corresponding to the $\pi-\pi^*$ signal of the aromatic carbon structure, indicated

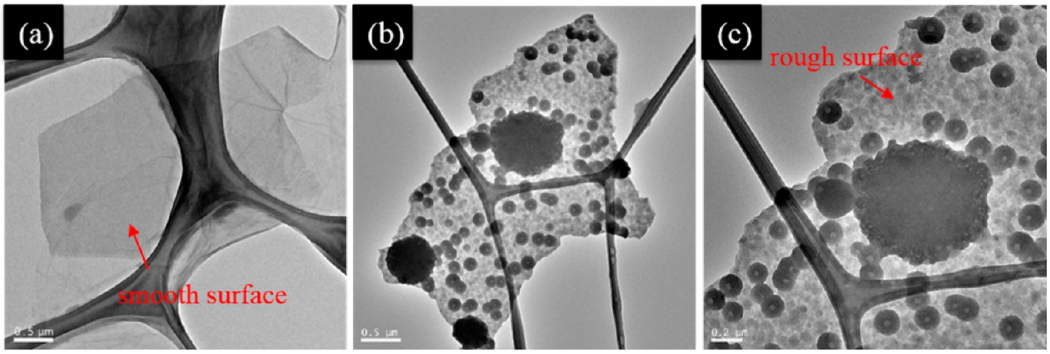

Figure 4. TEM images of (a) GO, (b) pGO, and (c) pGO at high magnification.

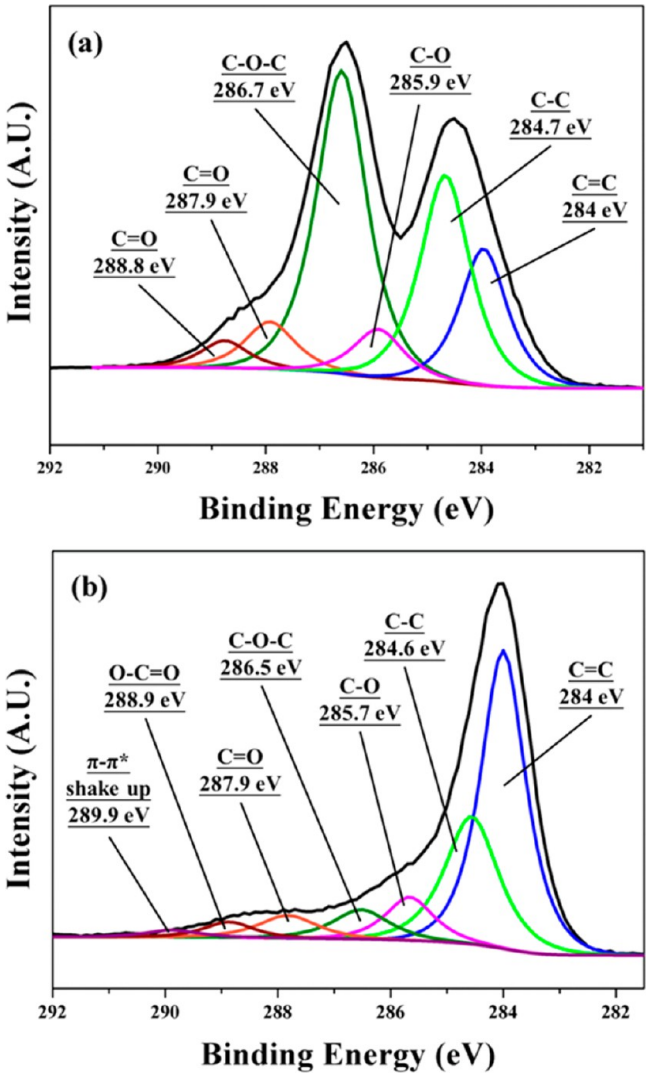

Figure 5. C 1s peaks in the XPS spectrum of (a) GO and (b) r-GO.

that the delocalized π conjugation had been restored after HI reduction. To further investigate the structure change during HI reduction, the Raman spectra of GO/WPU and r-GO/WPU composites were measured and are shown in the Supporting Information Figure S1. After reduction, the sharper G-band and smaller D-band of r-GO/WPU composites were observed, which demonstrated a more complete aromatic structure of r-GO/WPU composites than those of GO/WPU composites. In addition, the smaller I_D/I_G of r-GO/WPU composites than those of GO/WPU composites were obtained, indicating to lower defect contents of r-GO/WPU composite after HI treatment. These results indicated a high degree of GO reduction following the use of HI reduction.

3.3. Morphology and Structure of GO/WPU and r-GO/WPU Composites. As shown in Figure 6, neat WPU mat was

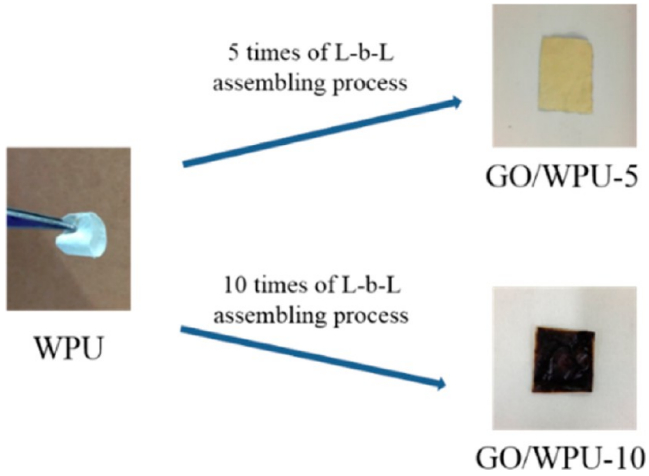

Figure 6. Photographs of WPU and GO/WPU composites captured after 5 and 10 cycles of L-b-L assembly.

white and flexible, but they became brownish after completing 5−10 cycles of L-b-L assembly, which indicated that the WPU fibers were successfully decorated with GO bilayers. The density of GO bilayers on the WPU fiber surfaces was related to the number of L-b-L-assembly cycles: after 5 cycles, small amounts of GO bilayers decorated the WPU fiber surface and GO/WPU-5 was light brown in color; however, after 10 cycles, the obtained GO/WPU-10 appeared dark brownish, indicating that the WPU fibers were completely decorated with GO bilayers.

We used SEM to further investigate the microstructure of the surface of the WPU fiber and GO/WPU composites (Figure 7). As shown in Figure 7a and b, WPU fibers exhibited a smooth surface and numerous pores. Figure 7c presented the microstructure of GO/WPU-10. The GO bilayers were decorated on the WPU fibers, and these GO bilayers formed connections that were guided by the WPU fibers. Moreover, GO/WPU-10 retained the original morphology of the WPU fiber, indicating that the structure of the WPU fiber did not crack during the process of L-b-L assembly. Furthermore, as shown in Figure 7d, the surface of the GO/WPU-10 composite GO/WPU-10 was rougher than that of the neat WPU fiber,

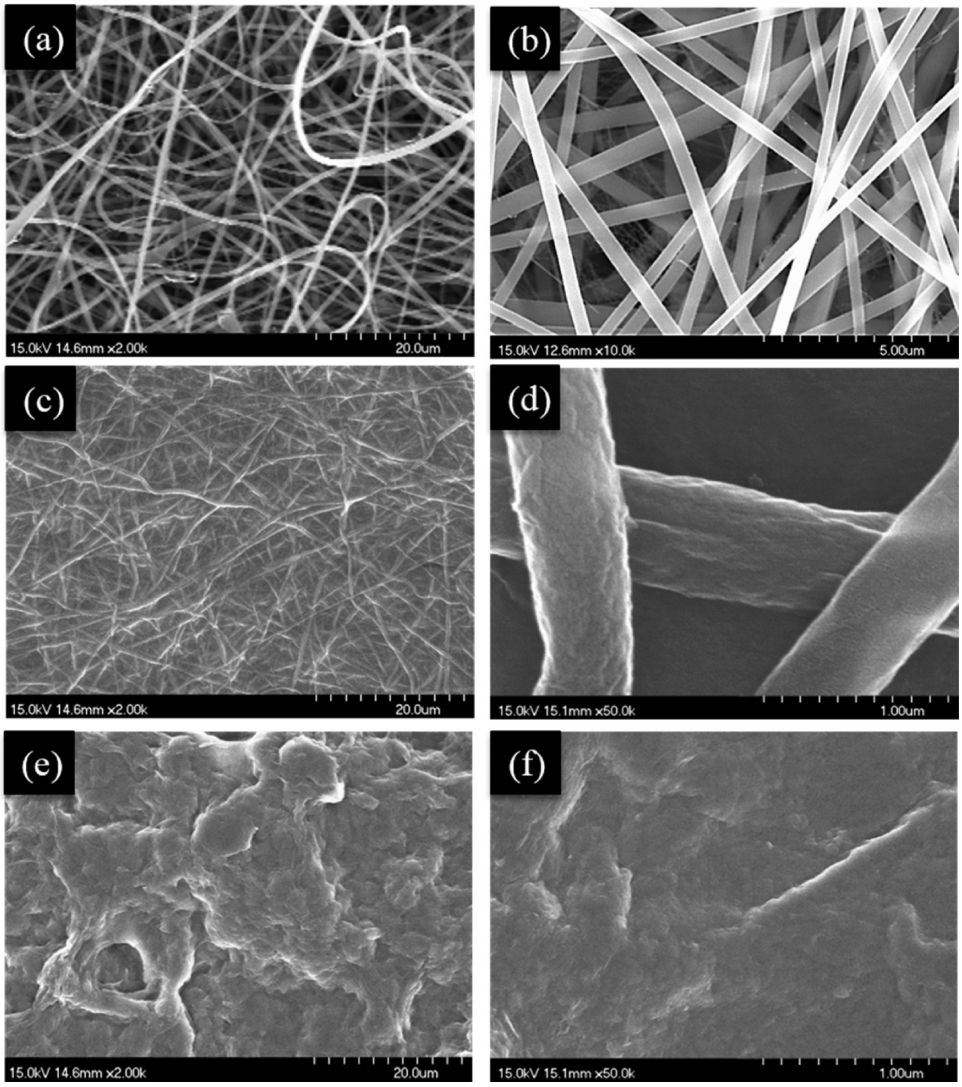

Figure 7. SEM images of surface of (a) WPU at low magnification (2 k), (b) WPU at high magnification (10 k), (c) GO/WPU-10 at low magnification (2 k), (d) GO/WPU-10 at high magnification (50 k), (e) GO/WPU-20 at low magnification (2 k), (f) GO/WPU-15 at high magnification (50 k).

indicating that GO bilayers wrapped the WPU fiber surface tightly by means of electrostatic interaction even after the fibers were rinsed using RO water. Lastly, after 20 cycles of L-b-L assembly, the WPU fibers were fully covered with GO bilayers and the pores among the WPU fibers were filled with GO bilayers; moreover, the amount of GO that lay over the WPU mat surface was too high to allow the underlying WPU fiber structure to be observed (Figure 7e and f).

HI were used to reduce GO to r-GO for restoring the structure and obtaining high electrical conductivity. A previous study[19] reported that the HI cannot break GO; however, WPU fibers were broken after treatment with HI (Figure 8a). Therefore, the performance of r-GO/WPU composites depended on the amount of r-GO that decorated the WPU fibers. As shown in Figure 8c, the GO/WPU-5 composites cracked when dipped in HI (red circles), and this was because the GO bilayers did not wrap the WPU fibers completely. The cracked WPU fibers obstructed the transfer of electrons among the r-GOs, which impeded the formation of the r-GO electrical conductive networks. Furthermore, the cracked WPU fibers did not exhibit high flexibility and mechanical properties. Figure 8b and d present a photograph and an SEM image of r-GO/WPU-10, which appeared black and was flexible. Because WPU fibers had been wrapped completely with GO bilayers after 10 cycles of L-b-L assembly, the result indicates that the wrapped GO bilayers protected the WPU fibers from cracking when dipped in HI, and that the wrapped GO bilayers were reduced to r-GOs. Moreover, the r-GO/WPU-10 composite retained the original WPU fiber structure, and the r-GOs remained tightly attached to the WPU fiber and had not peeled off during the reduction process (Figure 8e). Figure 8f and g present SEM images showing the morphology of r-GO/WPU-15. As in the case of GO/WPU-15, a thick r-GO layer decorated and tightly wrapped the WPU fibers (Figure 8g). Lastly, SEM images of r-GO/WPU-20 (Figure 8h and i) revealed that large quantities of r-GO lay over the WPU mat and that the WPU fiber could not be readily discerned, as in the case of GO/WPU-20.

The structures of WPU and r-GO/WPU composites were investigated by analyzing XRD patterns, as shown in Figure S2 in Supporting Information. WPU exhibited a broad diffraction peak at 20° indicating to the amorphous phase of WPU.[44,45] For the XRD patterns of r-GO/WPU composites, the

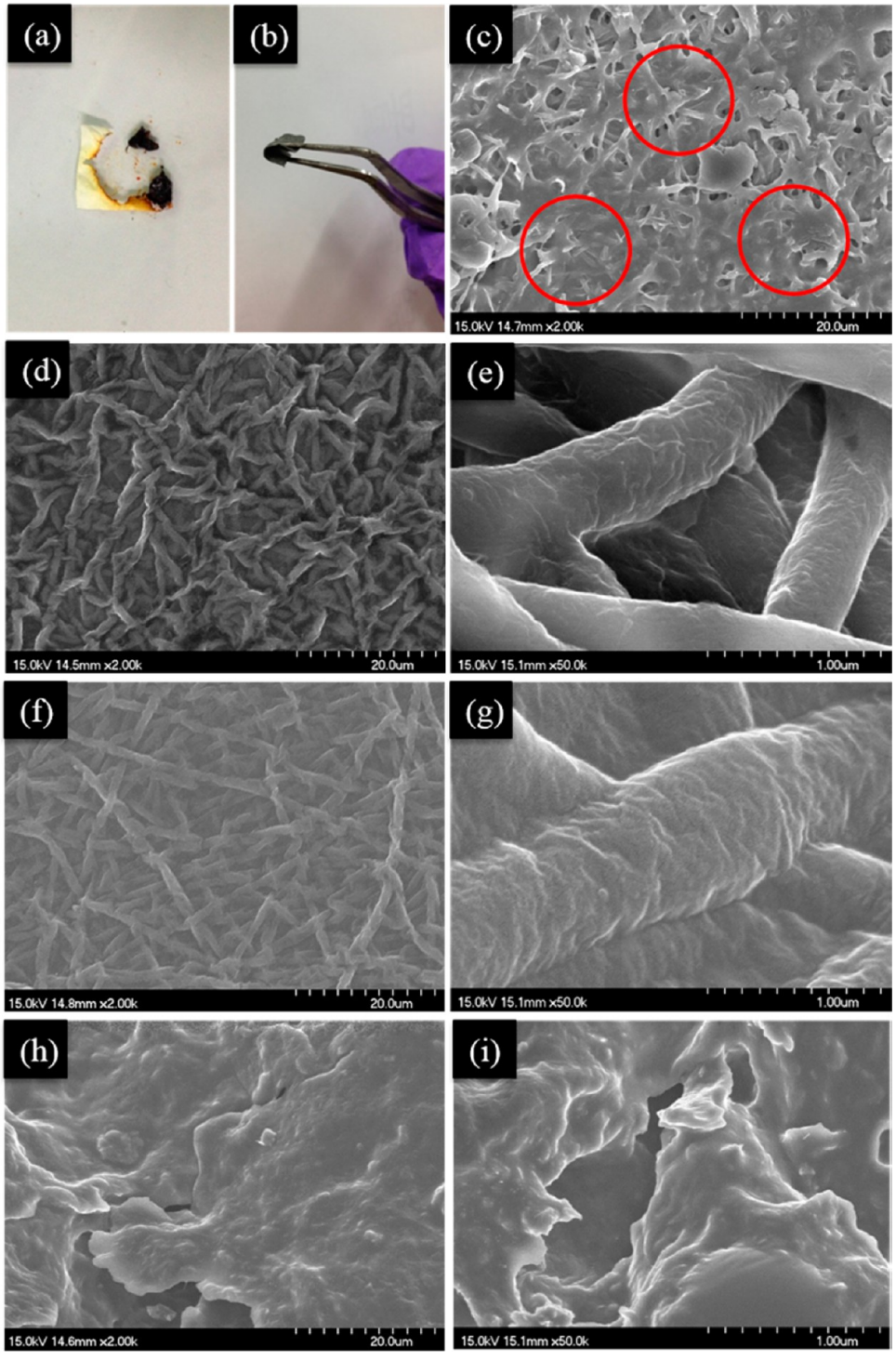

Figure 8. (a) Photographs of WPU with a drop of HI and (b) photographs of r-GO/WPU-15. (c) SEM images of r-GO/WPU-5, (d) SEM images of r-GO/WPU-10 at low magnification (2 k), (e) SEM images of r-GO/WPU-10 at high magnification (50 k), (f) SEM images of r-GO/WPU-15 at low magnification (2 k), (g) r-GO/WPU-15 at high magnification (50 k), (h) SEM images of r-GO/WPU-20 at low magnification (2 k), and (i) SEM images of r-GO/WPU-20 at high magnification (50 k).

characteristic diffraction peaks at 2θ = 24° were found corresponding to a d spacing of 0.37 nm, which was the (002) diffraction peak of r-GO.[19,46] The XRD analysis further indicated the r-GO decorated on the WPU fiber tightly.

3.4. TGA Analysis of r-GO, WPU, and r-GO/WPU Composites. Figure 9 presents the results of TGA investigations of WPU, r-GO, r-GO/WPU-10, and r-GO/WPU-15 composites. Highly thermal stable r-GO exhibited no significant weight loss. The weight ratio of the residues obtained for WPU, r-GO/WPU-10, and r-GO/WPU-15 were approximately 2.3%, 6.2%, and 9.5%, respectively. The weight ratios of the residues of the r-GO/WPU composites increased with increasing numbers of L-b-L assembly cycles.

Previous study[47] proposed a method to determine the weight fraction of r-GO adsorbed on the fibers: the total weight of r-GO/WPU composite is $m_t = m_g + m_f$; where m_g and m_f are the

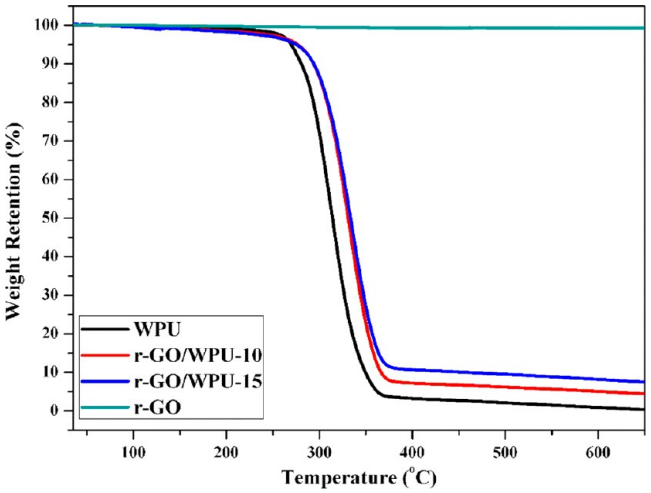

Figure 9. TGA curves for WPU, r-GO, r-GO/WPU-10, and r-GO/WPU-15.

weight of r-GO adsorbed on the WPU fibers and the WPU fibers, respectively. Then, combined with the TGA results of r-GO, WPU and r-GO/WPU-10 (at 500 °C), 6.2% $m_t = m_g +$ 2.3% m_f, the weight fraction of r-GO adsorbed on the WPU fiber of (m_g/m_t) r-GO/WPU-10 was calculated as about 4.2%, and that of r-GO/WPU-15 was also calculated to be about 7.5%.

Moreover, the TGA curves obtained for the r-GO/WPU composites were shifted toward higher temperatures than the curves obtained for WPU fibers, indicating enhanced thermal stability of the WPU matrix. According to the previous study,[48] the adsorbed r-GOs, which was highly thermal stable, can shield and dissipate heat efficiently, meanwhile, the adsorbed r-GOs can prevent the WPU fibers from thermal decomposition during ramping temperature, which can be supported by the TGA analysis with different ramping rate (Supporting Information Figure S3).

3.5. Electrical Properties of r-GO/WPU Composites. Figure 10 presents the electrical conductivity (σ) of r-GO/WPU composites as a function of the number of cycles of L-b-L assembly. Electrical conductivity increased with increasing cycles of L-b-L assembly in the case of r-GO/WPU-5, -7, -10, -12, -15, and -20. The r-GO/WPU composites with fewer numbers of cycles of L-b-L assembly (r-GO/WPU-1, -3, and -5) did not exhibited high electrical conductivity because the GO bilayers did not wrap the WPU fiber finely and the networks of electrical conduction were not constructed after the reduction. Moreover, the bare WPU fibers were broken by HI during reduction, which was shown by the SEM images (Figure 8c). The electrical conductivity of r-GO/WPU-10 increased to 7.03 S/m from the almost insulated GO/WPU composite (about 10^{-14} S/cm, Supporting Information Figure S4), indicating that the GO bilayers had been highly reduced, and conducted networks of r-GO had formed. After 15 cycles of L-b-L assembly, the electrical conductivity increased to 16.8 S/m. These enhancements indicated that complete networks of electrical conduction were constructed by the GO bilayers that wrapped the WPU fibers during the cycles of L-b-L assembly. Moreover, using HI effectively reduced GO to r-GO; meanwhile, the cationic surfactant on pGO was removed. However, after 20 cycles of L-b-L assembly, the electrical conductivity measured was lower than that of r-GO/WPU-15. This result revealed that the content of GO wrapped on the WPU fiber was extremely high, and that large amounts of GO bilayers lay over the WPU mat, which impeded HI reducing the GO bilayers that decorated the WPU fibers inside the WPU mat. This result agrees with our SEM investigation. To prove this demonstration briefly, the electrical conductivity of r-GO/WPU-20 was measured as a function of immersion time of HI treatment, as shown in Supporting Information Figure S5. The electrical conductivity of r-GO/WPU-20 has no significant increase with increased immersion time. The excess GO bilayers that were attached merely capped the surface of the WPU mat and were unable to form complete paths of electrical conduction. Thus, electrical conductivity decreased slightly when the cycles of L-b-L assembly was above 15 times, and r-GO/WPU-15 exhibited the highest electrical conductivity, of 16.8 S/m. Compared with the results of a previous study,[47] the r-GO/WPU composites exhibited high electrical conductivity coupled with low loading of r-GO (approximately 7.5 wt %). This result indicates that the high aspect ratios and random distribution of WPU fibers facilitated the construction of conductive networks. Moreover, the L-b-L assembly process avoided the aggregation of r-GOs and increased connectivity among r-GOs without junction resistance, and enabled formation of the conductive pathways.

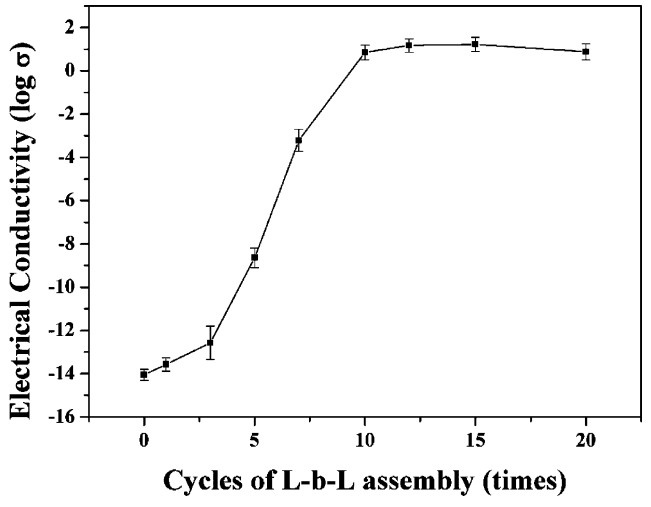

Figure 10. Electrical conductivity (σ) of r-GO/WPU composites measured at room temperature as a function of cycles of L-b-L assembly.

3.6. EMI Shielding Performance of r-GO/WPU Composites. The EMI SE of r-GO/WPU composites generated using various numbers of L-b-L-assembly cycles were measured over the frequency range of 8.2−12.4 GHz (Figure 11). The SE of a shielding material is commonly expressed in decibels (dB), with higher SE values suggesting the transmission of fewer electromagnetic waves that transmits through the shielding material. The WPU mat was almost transparent to electromagnetic waves and exhibited no shielding ability because of its insulating feature. After the L-b-L-assembly cycles and reduction using HI, the r-GO/WPU composites exhibited a high EMI SE, which increased with increasing numbers of L-b-L assembly cycles. The EMI SE of r-GO/WPU-10 was determined to be approximately 25 dB, and this rapid increase of SE in r-GO/WPU-10 occurred because the r-GOs formed networks of electrical conduction. After 15 cycles of L-b-L assembly, the SE reaches above 34 dB because the networks of

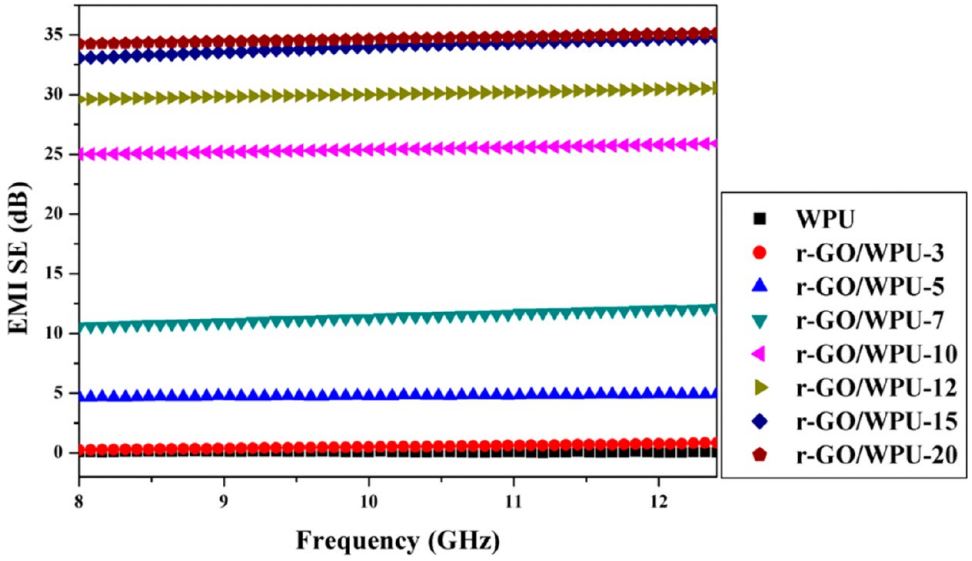

Figure 11. EMI SE of r-GO/WPU composites with various cycles of L-b-L assembly as a function of frequency in the range of 8.2−12.4 GHz (X band). The r-GO/WPU-15 exhibited EMI SE of approximately 34 dB in the range of 8.2−12.4 GHz.

electrical conduction formed were more complex than those in r-GO/WPU-10; this result also agrees with our SEM investigations and the measured trend of electrical conductivity. However, the EMI SE of r-GO/WPU-20 was only approximate 35 dB, which showed a lower enhancement than that of r-GO/WPU-15. As explained in the case of the electrical conductivity results, the large amounts of GO bilayers lay over the WPU mats prevented the penetration of HI to reduce the Go bilayers underneath and thus impeded the construction of the r-GO networks. The less completed electrical conductive network of r-GO/WPU-20 resulted in a limited enhancement of EMI SE.

As a result, r-GO/WPU-15 possessed the high EMI SE (34 dB) and featured only 7.5 wt % r-GO, which was much higher than the target value (∼20 dB) of EMI SE required for commercial application.[49] Supporting Information Table S1[4,5,22−25,49] summarizes the EMI SE of graphene-based composites reported by other researchers. It seemed that the EMI SE of r-GO/WPU composite used in this work is not very high compared to other composite. However, the thickness of the r-GO/WPU composite was only about 1 mm that was much smaller than other composites, 34 dB of such a thin thickness (1 mm) shielding material was an excellent value in the X-band region.

The mechanisms of EMI shielding was further investigated by plotting the SE_{total}, SE_A, and SE_R values of the r-GO/WPU composites as a function of the number of L-b-L-assembly cycles at 9 GHz (Figure 12). In the case of the r-GO/WPU-15 composite, the value of SE_{total}, SE_A, and SE_R were 34, 31, and 3 dB, respectively. The SE_A values at various cycles of L-b-L assembly were higher than SE_R values, which can be attributed to the EMI-shielding mechanism being dominated by absorption and showing a similar growth trend of SE_{total}. An incident electromagnetic wave is decayed by the conductive dissipation of shielding materials. High electrical conductivity and the completeness of the networks of electrical conduction play a key role in the EMI-shielding performance of composites.[5,6,50] Less complete r-GO conductive networks that increase intersheet junction contract resistance, which impeded the absorption loss. Here, the continued conductive paths were formed by r-GOs that wrapped on WPU fiber after

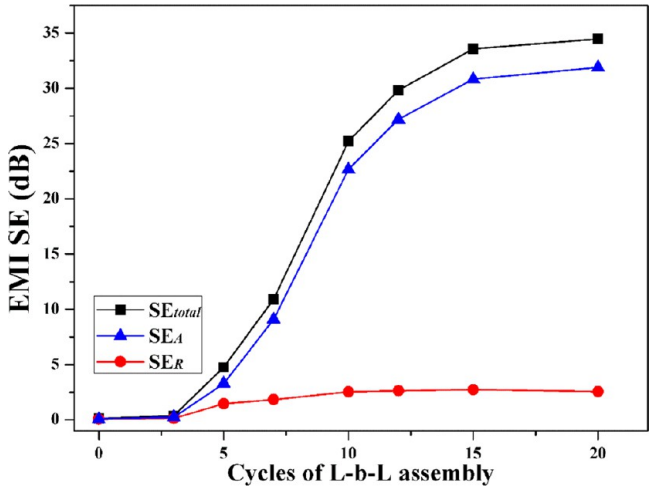

Figure 12. Comparison of SE_{total}, SE_A, and SE_R of r-GO/WPU composites as a function of cycles of L-b-L assembly at 9 GHz.

cycles of L-b-L assembly and reduced by HI, which was benefit for the absorption loss. In addition, r-GOs featuring large surface areas and interface areas in the r-GO/WPU composites also contribute toward increasing the probability of interacting with incident electromagnetic waves. Electromagnetic microwaves were difficult to escape from the r-GO/WPU composite, and the electromagnetic microwaves were absorbed and transformed into heat by the continuous r-GO networks. Here, the prepared r-GO/WPU composite exhibited a high EMI shielding performance in the absorption domain, this composite has a large potential as an EMI-shielding material.

4. CONCLUSION

In this study, the L-b-L assembly method described here is an effective approach to prepare GO/WPU composites, and HI efficiently reduced a substantial amount of GO to r-GO. The obtained r-GO/WPU composites exhibited high electrical conductivity (up to 16.8 S/m) and EMI SE (up to 34 dB), which is an excellent performance at such a thin thickness (1 mm). This simple and powerful approach enabled the

fabrication of r-GO/WPU composites that are lightweight and flexible and exhibited high electrical conductivity and EMI shielding performance, which enables potential as high-performance EMI shielding materials in flexible electronics, such as soft portable electronic products, roll-up displays, and health-monitoring electronic skins.

■ ASSOCIATED CONTENT

Supporting Information

Zeta potential characterization, figures showing Raman spectra, XRD results, TGA analysis, and electrical conductivity, and a table comparing EMI SI with GNS composites. This material is available free of charge via the Internet at http://pubs.acs.org.

■ AUTHOR INFORMATION

Corresponding Author

*Tel.: 886-3-5713058. Fax: 886-3-5715408. E-mail: ccma@che.nthu.edu.tw.

Notes

The authors declare no competing financial interest.

■ ACKNOWLEDGMENTS

The authors acknowledge the National Science Council, Taiwan for financially supporting this research (NSC 101-2221-E-007-031-(102), and NSC 102-2622-E-007-024-CC3).

■ REFERENCES

(1) Devender; Ramasamy, S. R. A Review of EMI Shielding and Suppression Materials. *Proc. Int. Conf. Electromagn. Interference. Compat.* **1997**, 459−466.

(2) Watts, P. C. P.; Hsu, W. K.; Barnes, A.; Chambers, B. High Permittivity from Defective Multiwalled Carbon Nanotubes in the X-Band. *Adv. Mater.* **2003**, *15* (7−8), 600−603.

(3) Li, N.; Huang, Y.; Du, F.; He, X. B.; Lin, X.; Gao, H. J.; Ma, Y. F.; Li, F. F.; Chen, Y. S.; Eklund, P. C. Electromagnetic Interference (EMI) Shielding of Single-Walled Carbon Nanotube Epoxy Composites. *Nano Lett.* **2006**, *6* (6), 1141−1145.

(4) Liang, J.; Wang, Y.; Huang, Y.; Ma, Y.; Liu, Z.; Cai, J.; Zhang, C.; Gao, H.; Chen, Y. Electromagnetic Interference Shielding of Graphene/Epoxy Composites. *Carbon* **2009**, *47* (3), 922−925.

(5) Zhang, H.-B.; Zheng, W.-G.; Yan, Q.; Jiang, Z.-G.; Yu, Z.-Z. The Effect of Surface Chemistry of Graphene on Rheological and Electrical Properties of Polymethylmethacrylate Composites. *Carbon* **2012**, *50* (14), 5117−5125.

(6) Chung, D. D. L. Electromagnetic Interference Shielding Effectiveness of Carbon Materials. *Carbon* **2001**, *39* (2), 279−285.

(7) Wang, L. L.; Tay, B. K.; See, K. Y.; Sun, Z.; Tan, L. K.; Lua, D. Electromagnetic Interference Shielding Effectiveness of Carbon-Based Materials Prepared by Screen Printing. *Carbon* **2009**, *47* (8), 1905−1910.

(8) Yang, Y.; Gupta, M. C.; Dudley, K. L.; Lawrence, R. W. Conductive Carbon Nanofiber−Polymer Foam Structures. *Adv. Mater.* **2005**, *17* (16), 1999−2003.

(9) Novoselov, K. S.; Geim, A. K.; Morozov, S. V.; Jiang, D.; Zhang, Y.; Dubonos, S. V.; Grigorieva, I. V.; Firsov, A. A. Electric Ffield Effect in Atomically Thin Carbon Films. *Science* **2004**, *306* (5696), 666−669.

(10) Stankovich, S.; Dikin, D. A.; Dommett, G. H. B.; Kohlhaas, K. M.; Zimney, E. J.; Stach, E. A.; Piner, R. D.; Nguyen, S. T.; Ruoff, R. S. Graphene-Based Composite Materials. *Nature* **2006**, *442* (7100), 282−286.

(11) Kim, H.; Abdala, A. A.; Macosko, C. W. Graphene/Polymer Nanocomposites. *Macromolecules* **2010**, *43* (16), 6515−6530.

(12) Stankovich, S.; Dikin, D. A.; Piner, R. D.; Kohlhaas, K. A.; Kleinhammes, A.; Jia, Y.; Wu, Y.; Nguyen, S. T.; Ruoff, R. S. Synthesis of Graphene-Based Nanosheets via Chemical Reduction of Exfoliated Graphite Oxide. *Carbon* **2007**, *45* (7), 1558−1565.

(13) Park, S.; Ruoff, R. S. Chemical Methods for the Production of Graphenes. *Nat. Nanotechnol.* **2009**, *4* (4), 217−224.

(14) Gao, W.; Alemany, L. B.; Ci, L. J.; Ajayan, P. M. New Insights Into the Structure and Reduction of Graphite Oxide. *Nat. Chem.* **2009**, *1* (5), 403−408.

(15) Dreyer, D. R.; Park, S.; Bielawski, C. W.; Ruoff, R. S. The Chemistry of Graphene Oxide. *Chem. Soc. Rev.* **2010**, *39* (1), 228−240.

(16) Kim, J.; Cote, L. J.; Kim, F.; Yuan, W.; Shull, K. R.; Huang, J. X. Graphene Oxide Sheets at Interfaces. *J. Am. Chem. Soc.* **2010**, *132* (23), 8180−8186.

(17) Wang, H.; Robinson, J. T.; Li, X.; Dai, H. Solvothermal Reduction of Chemically Exfoliated Graphene Sheets. *J. Am. Chem. Soc.* **2009**, *131* (29), 9910−9911.

(18) Shin, H. J.; Kim, K. K.; Benayad, A.; Yoon, S. M.; Park, H. K.; Jung, I. S.; Jin, M. H.; Jeong, H. K.; Kim, J. M.; Choi, J. Y. Efficient Reduction of Graphite Oxide by Sodium Borohydride and Its Effect on Electrical Conductance. *Adv. Funct. Mater.* **2009**, *19* (12), 1987−1992.

(19) Pei, S.; Zhao, J.; Du, J.; Ren, W.; Cheng, H.-M. Direct Reduction of Graphene Oxide Films into Highly Conductive and Flexible Graphene Films by Hydrohalic Acids. *Carbon* **2010**, *48* (15), 4466−4474.

(20) Kim, H.; Miura, Y.; Macosko, C. W. Graphene/Polyurethane Nanocomposites for Improved Gas Barrier and Electrical Conductivity. *Chem. Mater.* **2010**, *22* (11), 3441−3450.

(21) Zhang, H.-B.; Yan, Q.; Zheng, W.-G.; He, Z.; Yu, Z.-Z. Tough Graphene−Polymer Microcellular Foams for Electromagnetic Interference Shielding. *ACS Appl. Mater. Interfaces* **2011**, *3* (3), 918−924.

(22) Hsiao, S.-T.; Ma, C.-C. M.; Tien, H.-W.; Liao, W.-H.; Wang, Y.-S.; Li, S.-M.; Huang, Y.-C. Using a Non-covalent Modification to Prepare a High Electromagnetic Interference Shielding Performance Graphene Nanosheet/Water-Borne Polyurethane Composite. *Carbon* **2013**, *60* (0), 57−66.

(23) Ling, J.; Zhai, W.; Feng, W.; Shen, B.; Zhang, J.; Zheng, W. g. Facile Preparation of Lightweight Microcellular Polyetherimide/Graphene Composite Foams for Electromagnetic Interference Shielding. *ACS Appl. Mater. Interfaces* **2013**, *5* (7), 2677−2684.

(24) Yan, D.-X.; Ren, P.-G.; Pang, H.; Fu, Q.; Yang, M.-B.; Li, Z.-M. Efficient Electromagnetic Interference Shielding of Lightweight Graphene/Polystyrene Composite. *J. Mater. Chem.* **2012**, *22* (36), 18772−18774.

(25) Chen, Z.; Xu, C.; Ma, C.; Ren, W.; Cheng, H. M. Lightweight and Flexible Graphene Foam Composites for High-Performance Electromagnetic Interference Shielding. *Adv. Mater.* **2013**, *25*, 1296−1300.

(26) Hu, L.; Pasta, M.; Mantia, F. L.; Cui, L.; Jeong, S.; Deshazer, H. D.; Choi, J. W.; Han, S. M.; Cui, Y. Stretchable, Porous, and Conductive Energy Textiles. *Nano Lett.* **2010**, *10* (2), 708−714.

(27) Yu, G.; Hu, L.; Vosgueritchian, M.; Wang, H.; Xie, X.; McDonough, J. R.; Cui, X.; Cui, Y.; Bao, Z. Solution-Processed Graphene/MnO_2 Nanostructured Textiles for High-Performance Electrochemical Capacitors. *Nano Lett.* **2011**, *11* (7), 2905−2911.

(28) Alazemi, M.; Dutta, I.; Wang, F.; Blunk, R. H.; Angelopoulos, A. P. Electrically Conductive Thin Films Prepared from Layer-by-Layer Assembly of Graphite Platelets. *Adv. Funct. Mater.* **2009**, *19* (7), 1118−1129.

(29) WookáLee, D.; YoungáKim, J.; SukáShin, H. Highly Controllable Transparent and Conducting Thin Films Using Layer-by-Layer Assembly of Oppositely Charged Reduced Graphene Oxides. *J. Mater. Chem.* **2011**, *21* (10), 3438−3442.

(30) Shen, J.; Hu, Y.; Li, C.; Qin, C.; Shi, M.; Ye, M. Layer-by-Layer Self-Assembly of Graphene Nanoplatelets. *Langmuir* **2009**, *25* (11), 6122−6128.

(31) Tien, H.-W.; Huang, Y.-L.; Yang, S.-Y.; Hsiao, S.-T.; Wang, J.-Y.; Ma, C.-C. M. Graphene Nanosheets Deposited on Polyurethane Films by Self-Assembly for Preparing Transparent, Conductive Films. *J. Mater. Chem.* **2011**, *21* (38), 14876−14883.

(32) Tien, H.-W.; Huang, Y.-L.; Yang, S.-Y.; Hsiao, S.-T.; Liao, W.-H.; Li, H.-M.; Wang, Y.-S.; Wang, J.-Y.; Ma, C.-C. M. Preparation of Transparent, Conductive Films by Graphene Nanosheet Deposition

on Hydrophilic or Hydrophobic Surfaces Through Control of the pH Value. *J. Mater. Chem.* **2012**, *22* (6), 2545−2552.
(33) Hirata, M.; Gotou, T.; Horiuchi, S.; Fujiwara, M.; Ohba, M. Thin-Film Particles of Graphite Oxide 1: High-Yield Synthesis and Flexibility of the Particles. *Carbon* **2004**, *42* (14), 2929−2937.
(34) Hummers, W. S.; Offeman, R. E. Preparation of Graphitic Oxide. *J. Am. Chem. Soc.* **1958**, *80* (6), 1339−1339.
(35) Buruaga, L.; Sardon, H.; Irusta, L.; Gonzalez, A.; Fernandez-Berridi, M. J.; Iruin, J. J. Electrospinning of Waterborne Polyurethanes. *J. Appl. Polym. Sci.* **2010**, *115* (2), 1176−1179.
(36) Wang, J. C.; Xiang, C. S.; Liu, Q.; Pan, Y. B.; Guo, J. K. Ordered Mesoporous Carbon/Fused Silica Composites. *Adv. Funct. Mater.* **2008**, *18* (19), 2995−3002.
(37) Kim, H. M.; Kim, K.; Lee, C. Y.; Joo, J.; Cho, S. J.; Yoon, H. S.; Pejakovic, D. A.; Yoo, J. W.; Epstein, A. J. Electrical Conductivity and Electromagnetic Interference Shielding of Multiwalled Carbon Nanotube Composites Containing Fe Catalyst. *Appl. Phys. Lett.* **2004**, *84* (4), 589−591.
(38) Yuan, B.; Yu, L.; Sheng, L.; An, K.; Zhao, X. Comparison of Electromagnetic Interference Shielding Properties Between Single-Wall Carbon Nanotube and Graphene Sheet/Polyaniline Composites. *J. Phys. D: Appl. Phys.* **2012**, *45* (23), 235108.
(39) Li, D.; Müller, M. B.; Gilje, S.; Kaner, R. B.; Wallace, G. G. Processable Aqueous Dispersions of Graphene Nanosheets. *Nat. Nanotechnol.* **2008**, *3* (2), 101−105.
(40) White, B.; Banerjee, S.; O'Brien, S.; Turro, N. J.; Herman, I. P. Zeta-Potential Measurements of Surfactant-Wrapped Individual Single-Walled Carbon Nanotubes. *J. Phys. Chem. C* **2007**, *111* (37), 13684−13690.
(41) Liao, W. H.; Yang, S. Y.; Wang, J. Y.; Tien, H. W.; Hsiao, S. T.; Wang, Y. S.; Li, S. M.; Ma, C. C. M.; Wu, Y. F. Effect of Molecular Chain Length on the Mechanical and Thermal Properties of Amine-Functionalized Graphene Oxide/Polyimide Composite Films Prepared by In Situ Polymerization. *ACS Appl. Mater. Interfaces* **2013**, *5* (3), 869−877.
(42) Mattevi, C.; Eda, G.; Agnoli, S.; Miller, S.; Mkhoyan, K. A.; Celik, O.; Mastrogiovanni, D.; Granozzi, G.; Garfunkel, E.; Chhowalla, M. Evolution of Electrical, Chemical, and Structural Properties of Transparent and Conducting Chemically Derived Graphene Thin Films. *Adv. Funct. Mater.* **2009**, *19* (16), 2577−2583.
(43) Szabó, T.; Berkesi, O.; Forgó, P.; Josepovits, K.; Sanakis, Y.; Petridis, D.; Dékány, I. Evolution of Surface Functional Groups in a Series of Progressively Oxidized Graphite Oxides. *Chem. Mater.* **2006**, *18* (11), 2740−2749.
(44) Kim, B. K.; Seo, J. W.; Jeong, H. M. Morphology and Properties of Waterborne Polyurethane/Clay Nanocomposites. *Eur. Polym. J.* **2003**, *39* (1), 85−91.
(45) Lee, Y. R.; Raghu, A. V.; Jeong, H. M.; Kim, B. K. Properties of Waterborne Polyurethane/Functionalized Graphene Sheet Nanocomposites Prepared by An In Situ Method. *Macromol. Chem. Physic* **2009**, *210* (15), 1247−1254.
(46) Moon, I. K.; Lee, J.; Ruoff, R. S.; Lee, H. Reduced Graphene Oxide by Chemical Graphitization. *Nat. Commun.* **2010**, *1*, 73.
(47) Gao, J. F.; Hu, M. J.; Dong, Y. C.; Li, R. K. Y. Graphite-Nanoplatelet-Decorated Polymer Nanofiber with Improved Thermal, Electrical, and Mechanical Properties. *ACS Appl. Mater. Interfaces* **2013**, *5* (16), 7758−7764.
(48) Wu, Z.-S.; Ren, W.; Gao, L.; Zhao, J.; Chen, Z.; Liu, B.; Tang, D.; Yu, B.; Jiang, C.; Cheng, H.-M. Synthesis of Graphene Sheets with High Electrical Conductivity and Good Thermal Stability by Hydrogen Arc Discharge Exfoliation. *ACS Nano* **2009**, *3* (2), 411−417.
(49) Chen, M.; Zhang, L.; Duan, S.; Jing, S.; Jiang, H.; Luo, M.; Li, C. Highly Conductive and Flexible Polymer Composites with Improved Mechanical and Electromagnetic Interference Shielding Performances. *Nanoscale* **2014**, *6*, 3796−3803.
(50) Al-Saleh, M. H.; Sundararaj, U. Electromagnetic Interference Shielding Mechanisms of CNT/Polymer Composites. *Carbon* **2009**, *47* (7), 1738−1746.